11th International Conference on Fracture Mechanics of Concrete and Concrete Structures
FraMCoS-11
J. M. Chandra Kishen, A. Ramaswamy, S. Ray and R. Vidyasagar (Eds)
https://doi.org/10.21012/FC11.092376

DISCRETE MESOSCALE MODELLING OF CONCRETE USING DISCRETE EXTERIOR CALCULUS

PIETER D. BOOM[*†], MADYAN A. AL-SHUGAA[†] AND MUHAMMAD K. RAHMAN[†]

[*] Department of Mechanical Engineering,
King Fahd University of Petroleum and Minerals, Dhahran, Saudi Arabia
e-mail: pieter.boom@kfupm.edu.sa

[†] Interdisciplinary Research Center for Construction and Building Materials,
King Fahd University of Petroleum and Minerals, Dhahran, Saudi Arabia

Key words: Discrete exterior calculus, Voronoi tessellation, elastic-plastic, strain hardening, tensile fracture, finite element

Abstract: This paper investigates the application of discrete exterior calculus (DEC) to predict the material performance of concrete (mortar and aggregates). The aim is to simulate the discrete and heterogenous structure of concrete directly to better predict local phenomena and their impact on apparent global properties. Towards this goal, an existing DEC formulation of linear elasticity is extended to describe incremental elastic-plastic material behavior with isotropic strain hardening. A Voronoi tessellation of the physical domain is used to represent different constituents of the concrete, where each cell is assigned a local material model and material properties. The interaction of the cells is described using the Delaunay dual tetrahedralization of the tessellation. Constructing the mesh in this order required a new boundary closure for the DEC formulation, which is also presented herein. The formulation is validated through simulation and compared to finite element analysis obtained from Abaqus. Simulations include compression of cubical specimens composed of 1) mortar with uniform properties and elastic-plastic response; 2) mortar, as before, but with different volume fractions of aggregate added, having purely elastic response; as well as 3) some initial simulations with the formation of cracks from specimens in tension. Excellent results are obtained when compared to the finite-element analysis, laying the foundation to simulate more complex phenomena in the future.

1 INTRODUCTION

The discrete, heterogeneous, and spatially varying structure of concrete influences both its local and apparent global properties, as well as its response to applied loads – especially as these structures evolve. A mechanical example is the type, volume fraction, size, and arrangement of aggregates, which has a significant impact on stress response at subcritical loads and the dynamics of cracks beyond these limits [1-4]. Applied loads can also be interpreted to include the response of the material is multiphysics processes like thermal, chemical, electrical, or fluid processes [5-8].

The key structures that influence the material response of concrete are often well above the atomic scale, but do not globally satisfy the continuum assumption. While there are many different approaches to modelling concrete with continuum methods like finite elements – such as experimentally validated empirical models [9], remeshing [10], meshing multiple constituent domains individually [11], etc – they cannot represent the underlying physics from first principles.

Discrete exterior calculus (DEC) is a fundamentally discrete approach that uses the geometry and topology of a cell complex to describe the evolution of local properties and physical

processes [12,13]. Bypassing a global continuum assumption, this approach can naturally capture the impact of structure, heterogeneity, and discontinuities [14-17]. Beginning with a cell complex to represent material structure, creates natural paths for discontinuities (topological changes) to emerge and evolve. DEC also enables physical phenomena to evolve differently on lower dimensions skeletons of the cell complex. For example, processes like diffusion or fracture mechanics can be defined differently within the cell, across a face, or along an edge. It can also help model constituents that can be considered lower-dimensional objects, such as fibers or particulates.

Previously, DEC has been applied to predict linear elastic behavior and validated for Poisson's ratios from -0.95 to 0.45 for a variety of canonical mechanical problems [18]. This was inspired by the ideas presented in Ref. [19]. In this formulation, displacements are a vector-valued 0-cochain representing the movement of cell centers. The interaction between cells is described on the edge connecting the two cell centers - a discrete displacement gradient 1-cochain. The local cell-by-cell constitutive relationships are imposed through a non-diagonal material Hodge star, resulting in a 2-cochain on the faces of each cell – discrete forces. Finally, the balance of linear momentum is enforced at cell centers, once again as 0-cochain.

The goal of this paper is to extend the existing formulation of linear elasticity using DEC to simulate elastic-plastic behavior with isotropic hardening. The aim is to build up the capabilities of the theory and software implementation to study the mechanical performance of concrete relative to its inherent discrete structure, especially as it begins to degrade and fail. To validate the model, simulations will be presented in the elastic and plastic region, as well as some initial simulations with tensile fracture.

This paper is organized as follows: Section 2 presents a brief review of an existing formulation of linear elasticity using DEC, the extension to elastic-plastic behavior with isotropic strain hardening and a new boundary closure. Numerical simulations and a comparison with Abaqus finite element software [20] are then presented in Section 3. Finally, conclusions are drawn in Section 4.

2 PREDICTION OF MATERIAL PERFORMANCE USING DISCRETE EXTERIOR CALCULUS

In this paper, the underlying theory and notation of discrete exterior calculus (DEC) are based on Refs. [12,13] and the formulation of linear elastic material behavior based on Ref. [18]. Here a brief overview of the DEC approach is given, highlighting the new extension to plasticity, and a new boundary closure is presented.

2.1 Basic formulation

To begin, consider a physical specimen occupying the domain Ω. To predict the mechanical performance of the specimen using DEC, the domain is first tessellated with Voronoi cells. If the specimen has a material structure, the cells are created to coincide with that structure. For example: at longer length scales this could be used to represent aggregates, fibers, or rebar in a cement mortar, or at shorter length scales it could represent sand particles or small voids in a cement paste.

With the tessellation in hand, a material model and material properties matching the local conditions are then assigned to each cell. These are assumed constant within each cell, and potentially vary discontinuously from one cell to another. In the same way, the interface between cells can also be assigned different models and properties to describe how the cells interact. This could be used, for example, to represent an interfacial transition zone (ITZ).

Associated with Voronoi tessellation is a dual Delaunay tetrahedralization. This dual mesh is used in DEC to describe the interaction of the Voronoi cells. Therefore, the primary unknown is chosen to be a vector-valued 0-cochain of displacements at vertices in the Delaunay tetrahedralization (the cell centers of the Voronoi tessellation):

$$(displacements) = \mathrm{u}^{\star 0} \qquad (1)$$

A discrete displacement gradient is then computed with a dual vertex-edge boundary operator (a discrete exterior derivative). This produces a vector-valued 1-cochain on edges in the Delaunay tetrahedralization, the edges connecting adjacent Voronoi cell centers. Depending on the application, this can be used to represent the total strain or the incremental strain. The latter is used in this paper:

$$\epsilon^{\star 1} = d^{\star 0}\Delta \mathrm{u}^{\star 0} \tag{2}$$

At this point the constitutive relationship is applied using a non-diagonal material Hodge star, producing discrete stresses on the faces between adjacent Voronoi cells (a primal vector-valued 2-cochain). In this paper we use τ to denote stress since σ has a special meaning in DEC:

$$\tau^2 = \star^{\star 1}_{\mathrm{mat}}\, \epsilon^{\star 1} \tag{3}$$

Formally, the material Hodge star is composed of a discrete sharp musical isomorphism to the center of each Voronoi cell, the application of the constitutive relationship cell-by-cell, a discrete flat musical isomorphism back to edges, and finally a geometric diagonal Hodge star to the faces of the Voronoi tessellation:

$$\tau^2 = \underbrace{\star^{\star 1}_{\mathrm{geo}}\, \flat^{\star 1} P \#^{\star 1}}_{\star^{\star 1}_{\mathrm{mat}}}\, \epsilon^{\star 1} \tag{4}$$

Previously it was found to be advantageous to decompose the application of the constitutive relationship into components related to shape change and the combination of volume change and rotation [18]:

$$P = \underbrace{2\mu I}_{\text{shape}} + \underbrace{\tilde{P}}_{\text{vol/rot}} \tag{5}$$

This eliminates the need for approximate discrete musical isomorphisms in the important shape change component of the constitutive relationship. This is justified because the flat and sharp are inverse transformations in the continuous theory:

$$\begin{aligned}\tau^2 =& \star^{\star 1}_{\mathrm{geo}} \left(2\mu \flat^{\star 1} I \#^{\star 1}\right. \\ &\left. + \flat^{\star 1} \tilde{P} \#^{\star 1}\right) \epsilon^{\star 1} \\ \approx& \star^{\star 1}_{\mathrm{geo}} \left(2\mu + \flat^{\star 1} \tilde{P} \#^{\star 1}\right) \epsilon^{\star 1}\end{aligned} \tag{6}$$

Finally, once the discrete stresses have been computed on Voronoi faces, the balance of momentum in each cell is computed using the divergence. This is done using the face-cell boundary operator for the Voronoi tessellation (another discrete exterior derivative). This boundary operator conveniently ends up being the transpose of the boundary operator used previously. Body forces can also be added at this point if need be:

$$\begin{aligned} d^2 \tau^2 + \mathrm{f}^3 &= 0 \\ (d^{\star 0})^T \tau^2 + \mathrm{f}^3 &= 0 \end{aligned} \tag{7}$$

2.2 Extension to plasticity

Initially, the fourth-order tensors describing the constitutive relationship $(P, \tilde{P})$ are linear elastic $(P_{el}, \tilde{P}_{el})$. The applied strain is increased incrementally until the equivalent total stress in one or more cells in the tessellation exceeds its locally defined yield stress [21]:

$$\tau^{\star 0}_{eq} = \sqrt{\frac{3\tau^{\star 0}_{dev,i,j}\tau^{\star 0}_{dev,i,j}}{2}} > \tau_{\mathrm{yield}} \tag{8}$$

where

$$\tau^{\star 0}_{dev,i,j} = \left(1 - \frac{\delta_{i,j}}{3}\right)\tau^{\star 0}_{i,j}, \tag{9}$$

$$\tau^{\star 0} = \tau^{\star 0}_{\mathrm{initial}} + P \#^{\star 1} \epsilon^{\star 1} \tag{10}$$

Previously, the DEC formulation was only validated up to this point. Now, we extend the formulation to include plasticity. The constitutive relationship $(P, \tilde{P})$ here now follows the Prandtl-Reuss model [22] with the Von Mises yield surface and isotropic strain hardening:

$$\begin{aligned} P &= P_{el} + P_{pl} \\ P &= P_{el} - \frac{2\mu}{S}\tau^{\star 0}_{dev,i,j}\tau^{\star 0}_{dev,k,l} \end{aligned} \tag{11}$$

or

$$\tilde{P} = \tilde{P}_{el} + \tilde{P}_{pl}$$

$$\tilde{P} = \tilde{P}_{el} - \frac{2\mu}{S}\tau^{\star 0}_{dev,i,j}\tau^{\star 0}_{dev,k,l} \tag{12}$$

where

$$S = J_2^{\star 0}\left(1 + \frac{H}{2\mu}\right) \tag{13}$$

$$J_2^{\star 0} = \tau^{\star 0}_{dev,i,j}\tau^{\star 0}_{dev,i,j} \tag{14}$$

$$H = \frac{\partial}{\partial \epsilon_p^{\star 0}}\sqrt{\frac{J_2^{\star 0}}{3}} \tag{15}$$

$$\epsilon_p^{\star 0} = \sqrt{\frac{2}{3}\epsilon^{\star 0}_{p,i,j}\epsilon^{\star 0}{}_{p,i,j}} \tag{16}$$

This model is often used to predict the performance of metals, therefore in the future a Drucker-Prager model [23], which is more commonly used for concrete, will also be implemented.

2.3 Boundary closure

In the original application of DEC for linear elasticity [18], the Voronoi tessellation of the domain was computed as a byproduct of the Delaunay tetrahedralization. This required a closure to account for Voronoi cells at the boundary that were truncated (incomplete).

In this paper, the Voronoi tessellation is computed directly from the domain of the specimen under consideration. This requires a different boundary closure. In this case, it is because the Delaunay edges at the boundary are truncated (incomplete), rather than the Voronoi cells. A two-dimensional depiction is given in Figure 1. In other words, the boundary edges connect the center of a boundary Voronoi cell and extend toward the boundary, but do not have a cell outside the domain to connect to at the other end. This means that discrete displacement gradient and the discrete flat musical isomorphisms are ill defined at the boundary.

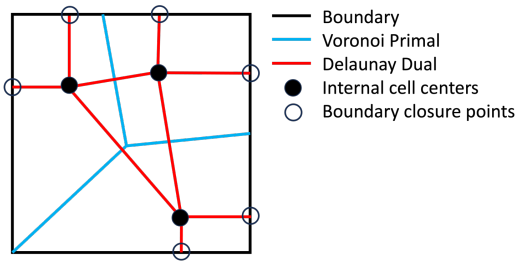

Figure 1: Depiction of truncated (incomplete) edges in the dual Delaunay triangularization and the additional points added to close the model.

To close the model, additional displacements are added to the centers of Voronoi faces on the boundary. This is similar in principle to the approach taken in Ref. [24]. The discrete displacement gradient is then computed between the displacements of the boundary cell and its boundary face. This too is shown in Figure 1.

The discrete flat musical isomorphism is also modified at the boundary to take values of the boundary Voronoi cell and project it along the truncated Delaunay edge extending to the boundary. This is consistent with the piecewise line integration used elsewhere in the mesh to compute the discrete flat.

Overall, the new approach allows the use of a more useful and complete tessellation directly, and is simpler than the previous closure in theory and implementation.

The final system that is solved is then in the following form:

$$\begin{bmatrix}\text{balance of momentum}\\ \text{surface forces}\end{bmatrix} = \begin{bmatrix}(d^{\star 0})^T\\ (d^{\star 0}_{\text{surf}})^T\end{bmatrix} \star^{\star 1}_{\text{geo}} \tilde{\flat}^{\star 1} P \#^{\star 1} \tag{17}$$

$$\begin{bmatrix} d^{\star 0} & d^{\star 0}_{\text{surf}}\end{bmatrix}\begin{bmatrix}\text{u}^{\star 1}\\ \text{u}^{1}_{\text{surf}}\end{bmatrix}$$

This is a square system that describes the mechanical behavior of the specimen under investigation. In this form, it is evident how to define both displacement and force boundary conditions. This will also reduce the size of the system that needs to be solved.

3 NUMERICAL RESULTS AND DISCUSSION

To demonstrate the performance of the extended DEC approach and new boundary closure, a series of simulations are presented with increasing complexity. The Voronoi tessellations are generated using Neper [25] and the numerical implementation of the theory is built on top of the MATLAB library presented [15]. The simulations presented here are for the compression tests on cubic specimens, first for a cube of uniform cement mortar, and then a cube of mortar with aggregates. Finally, some initial simulations are presented for specimens in tension which fail due to crack initiation and propagation. The boundary conditions applied in these simulations are prescribed displacements in the z-direction, and fixed displacements in the x- and y-directions on the z-min and z-min surfaces. The remaining 4 sides are free surfaces (zero forces).

Where possible, the results are compared with simulations results from Abaqus [20] (Finite elements). For the present simulations, we expect to get very close agreement between the two methods, as most end before the onset of major damage would occur. This is important as the current DEC formulation has no real damage model, except for the ability to fracture surfaces that exceed some tensile strength. In the future, the expectation is to simulate damage with the DEC formulation relative to the material structure, rather than implementing an empirical damage model.

3.1 Mortar only (homogeneous material)

The simplest case is to simulate pure mortar with uniform properties. This does not account for any microscale structure with sand, voids, etc – it models the material as a continuum. Previously, the DEC formulation has been validated in the elastic region for Poisson's ratios from -0.95 to 0.45 [18]; therefore, the focus here is on the plastic region. The material properties used for these simulations are as follows (Based on Ref. [1]):

$$E = 42.8GPa, \qquad \nu = 0.2$$

$$\tau_{\text{yield}} = 39.9MPa$$

The stress response of the uniform blocks up to 0.2% strain are shown in Figure 2, both with (right) and without (left) isotropic strain hardening. Positive stresses and strains are to be interpreted here as compressive stress. The meshes used are a regular orthogonal tessellation (top) and a quasi-random tessellation (bottom), both with 1000 cells. The meshes are shown in Figure 3.

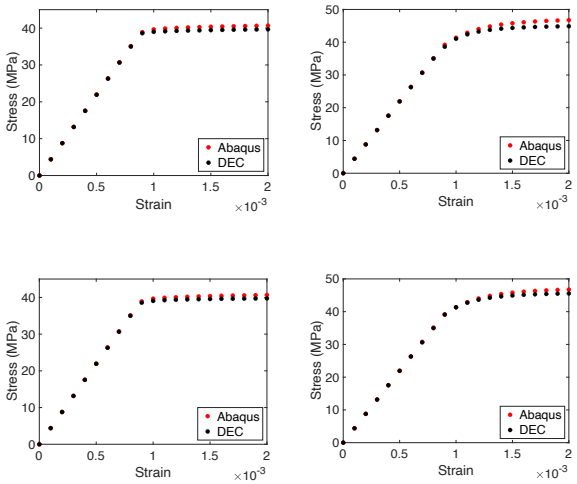

Figure 2: Stress-strain curves of mortar only. Top: regular orthogonal mesh; Bottom: quasi-random mesh; Left: pure plasticity; Right: Isotropic hardening.

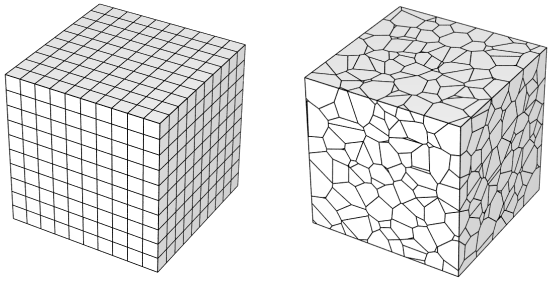

Figure 3: Meshes with 1000 cells.

As expected, the results for pure plasticity are linearly increasing in the elastic region, then are nearly horizontal in the plastic region. In the case of isotropic hardening, the figures show a more gradual flattening out of the curves and a higher maximum stress. This is

consistent with the growth of the yield surface due to the hardening.

Results generated with Abaqus are plotted in the same figure. The Abaqus results were generated with about 230,000 linear tetrahedrons, as shown in Figure 4. Relative to the Abaqus results, the DEC formulation slightly under-predicts the maximum stress both in the case with and without hardening. For pure plasticity, the maximum stress of the Abaqus results at 2% strain is about 40.65 MPa, whereas in DEC it remains about 39.7MPa – the yield stress being 39.9MPa. The DEC results remain around 39.7 all the way up to 5% strain.

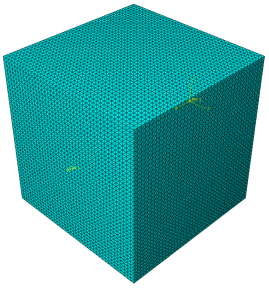

Figure 4: Abaqus mesh with ~230,000 tetrahedrons.

The stress fields of all three normal stresses and the xz-shear stresses are plotted in Figures 5-7, obtained from both the DEC formulation (regular orthogonal and quasi-random meshes) and Abaqus. In this case, compressive stress is computed as a negative value. Furthermore, finer meshes are used to get a closer plotting resolution to Abaqus, with approximately 8000-9000 cells. The results are from 0.2% strain with isotropic strain hardening and taken from one of the vertical mid-planes of the specimen. The figure shows excellent agreement in both stress magnitudes and patterns compared with the FEA.

3.2 Mortar and aggregate (heterogeneous material)

Increasing the complexity of the simulations, aggregates are now added to create a concrete cube. This is done by assigning a different material model and material properties to Voronoi cells selected to represent the

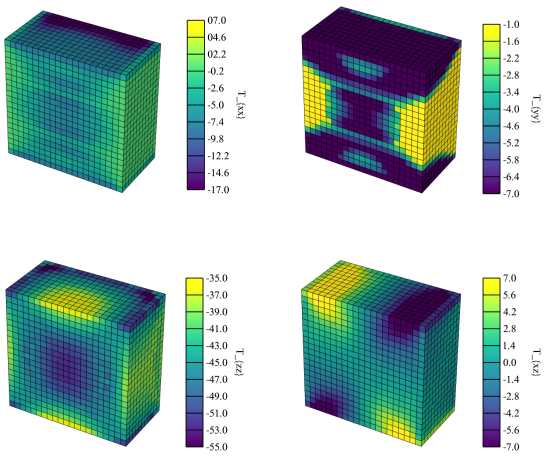

Figure 5: Stress distribution in the block at 0.2% strain using DEC on regular orthogonal mesh.

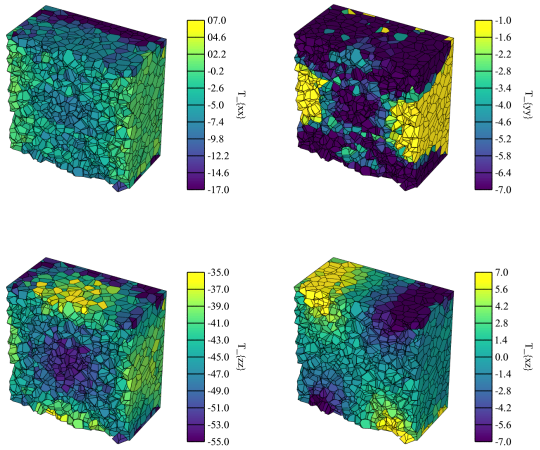

Figure 6: Stress distribution in the block at 0.2% strain using DEC on quasi-random mesh.

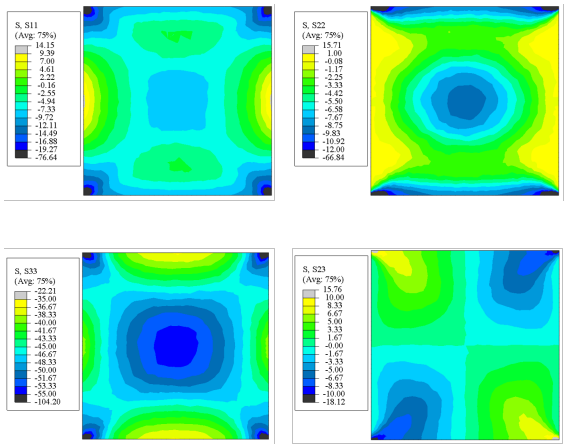

Figure 7: Stress distribution in the block at 0.2% strain using Abaqus.

aggregates. In this case, the aggregates are assumed to be elastic throughout the simulation range, and have the following material properties (Based on Ref. [1]):

$$E = 70GPa, \qquad \nu = 0.2$$

It is assumed that mortar cells have the same elastic-plastic response with isotropic hardening and the same material properties as before.

Figure 8 shows the variation in stress-strain obtained by adding different volume fractions of aggregates. Note that this approach allows for aggregates to be adjacent to one another and assumes that the mortar and aggregates are perfectly bonded. In the future, different interface characteristics will be implemented to simulate the ITZ. As expected, the addition of an increasing volume fraction of aggregates increases the maximum strength of the specimen.

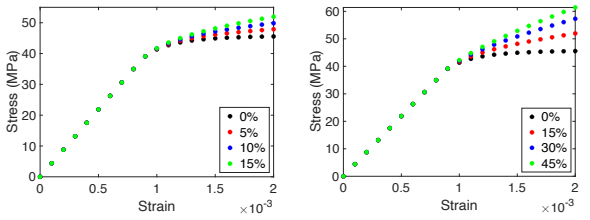

Figure 8: Stress-strain curve of cement mortar with different volume fractions of aggregates.

Figure 9 shows a comparison of the zz-normal stress field with (bottom) and without (top) the inclusion of a 15% volume fraction of aggregates using meshes with 1000 (left) and 8000 (right) cells. While the volume fractions are the same, the aggregate size is different using the two meshes. The figure highlights the higher compressive load carried by the aggregates, which was previously seen in the stress-strain curves (Figure 8), as well as the localized reaction of the aggregates enabled by the discrete approach.

3.3 Mortar and aggregate with cracks (discontinuous material)

To assess the ability of the discrete approach to introduce and propagate cracks, the DEC formulation is applied to the same concrete cubes, but now in tension. The properties of the mortar and aggregates remain the same, with the addition of a maximum tensile strength for the mortar (Based on Ref. [1]):

$$\tau_{tensile} = 3.9MPa$$

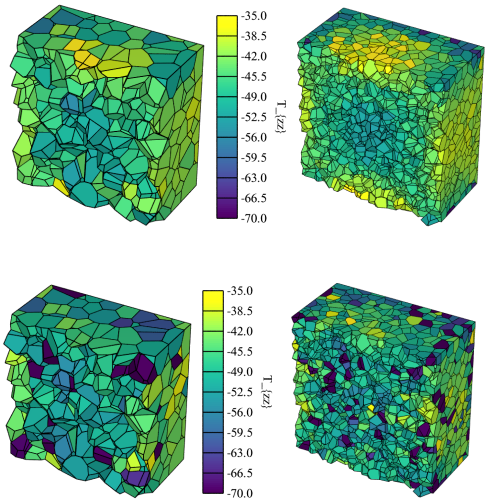

Figure 9: Stress field with (Bottom) and without (Top) a 15% volume fraction of aggregates. Left: 1000 cell mesh; Right: 8000 cell mesh

The tensile strength is interpreted here as a local property, rather than a global property. As the tensile stress at Voronoi faces in the mesh exceeds the tensile strength of the mortar, they are assumed to fail. Once the face fails, the material model is changed so that no load is supported in tension between the two adjacent cells. This is accomplished by zeroing the appropriate two values in the vertex-edge boundary operator defining the displacement gradient. By extension, this also zeroes the stress on the face and eliminates the contribution of the face to the balance of momentum.

The stress-strain curve for pure mortar is shown in Figure 10 and a sample fracture surface is shown in Figure 11. As expected, the tensile strength of the concrete block is much lower in tension than it was in compression. In this setup of the simulation, the maximum tensile stress occurs near the loading surfaces. However, the fractures were only allowed to occur within the block and not at the exterior boundaries. As expected, after a few faces fail, a growing fracture surface develops – in this case near the upper surface. The fracture

surface is approximately horizontal, failing along existing interfaces in the Voronoi tessellation.

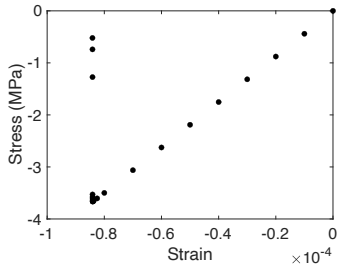

Figure 10: Stress-strain curve of mortar block in tension.

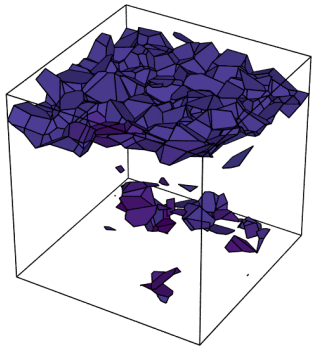

Figure 11: Fracture surface at failure of concrete block in tension.

4 CONCLUSIONS

This article presented an extended formulation of mechanical behavior using discrete exterior calculus (DEC) to study incremental elastic-plastic materials with isotropic strain hardening.

The extended formulation uses a Voronoi tessellation of the domain as the primal mesh and the Delaunay tetrahedralization as the dual. In contrast to previous work, the Voronoi tessellation is computed first, rather than a byproduct of a tetrahedralization, which enables more useful tessellations. This, however, necessitated a new boundary closure to account for truncated Delaunay edges at the boundary of the geometry. The new boundary closure places additional points at the center of Voronoi faces where the Delaunay edges truncate. These are accounted for in the formulation by modifying the boundary operator (discrete exterior derivatives) and discrete flat musical isomorphism. The new closure is in many ways simpler, both in theory and implementation, compared to the previous approach.

Validation of the new method was presented as a series of increasingly complex simulations, with results compared to Abaqus (finite elements). The first simulation was of mortar only, with uniform properties. The plastic response of a cubical specimen under compression was simulated, with very good agreement with Abaqus in terms of both local and global stress response.

Aggregates were then added to the mortar matrix, creating a mixture of materials with different properties and material models (aggregates were simulated as elastic only). The expected increase in global material strength was observed, as well as the local discrete response afforded by DEC.

Finally, a simulation of a concrete block in tension was presented to demonstrate the ability of the approach to simulate fracture. While this is a simple, and somewhat contrived simulation, it highlights the potential of the approach to be extended further and applied to more complex fracture mechanics of concrete structures in the future.

ACKNOWLEDGEMENTS

The authors would like to thank King Fahd University of Petroleum and Minerals Interdisciplinary Research Center for Construction and Building Materials (KFUPM IRC-CBM), Saudi Arabia, for supporting this investigation through Project No. INCB2313.

REFERENCES

[1] Jin, l., Wang, T., Jiang, X., Du, X., 2019. Size effect in shear failure of RC beams with stirrups: Simulation and formulation. *Eng. Struc.* **199:**109573

[2] Thilakarathna, P.S.M., Kristombu Baduge, K.S., Mendis, P., Vimonsatit, V., Lee, H., 2020. Mesoscale modelling of concrete – A review of geometry generation, placing algorithms, constitutive relations and applications. *Eng. Frac. Mech.*

231:106974,

[3] Chen, H., Xu, b., Mo, Y.L., Zhou, T., 2018. Behavior of meso-scale heterogeneous concrete under uniaxial tensile and compressive loadings. *Const. and Build. Mat.* **178:**418-431

[4] Zhou, Y., Jin, H., Wang, B., 2019. Modeling and mechanical influence of meso-scale concrete considering actual aggregate shapes, *Const. and Build. Mat.* **228:**116785

[5] Wang, L., Ueda, T., 2009. Meso-scale modeling of chloride diffusion in concrete with consideration of effects of time and temperature. *Water Sci. and Eng.* **2(3):**58-70

[6] Wang, L., Ueda, T., 2011. Mesoscale Modelling of the Chloride Diffusion in Cracks and Cracked Concrete. *J. of Adv. Concrete Tech.* **9(3):**241-249

[7] Asadi, I., Shafigh, P., Bin Abu Hassan, Z.F., Binti Mahyuddin, N., 2018. Thermal conductivity of concrete – A review. *J. of Build. Eng.* **20:**81-93

[8] Liang, M., Feng, K., He, C., Li, Y., An, L., Guo, W., 2020. A meso-scale model toward concrete water permeability regarding aggregate permeability. *Const. and Build. Mat.* **261:**120547

[9] Lee, J., Fenves, G., 1998. Plastic-Damage Model for Cyclic Loading of Concrete Structures. *J. Eng. Mech.* **124(8):**892-900

[10] Bouchard, P.O., Bay, F., Chastel, Y., Tovena, I., 2000. Crack propagation modelling using an advanced remeshing technique. *Comp. Meth. In App. Mech. and Eng.* **189(3):**723-742

[11] Jin, H., Zhou, Y., Wang, B., Zhou, S., 2018. Mesoscopic Finite Element Modeling of Concrete Considering Geometric Boundaries of Actual Aggregates. *Adv. In Mat. Sci. and Eng.* **2018:**7816502

[12] Hirani, A.N., 2003. Discrete exterior calculus, *Ph.D. thesis*, USA, AAI3086864.

[13] Desbrun, M., Hirani, A.N., Leok, M., Marsden, J.E., 2005. Discrete exterior calculus. *arXiv:math*/0508341.

[14] Boom, P.D., Jivkov, A.P., Margetts, L., 2023. ParaGEMS: Integrating discrete exterior calculus (DEC) into ParaFEM for geometric analysis of solid mechanics. *SoftwareX.* **21:**101280

[15] Berbatov, K., Boom, P.D., Hazel, A.L., Jivkov, A.P., 2022. Diffusion in multi-dimensional solids using Forman's combinatorial differential forms, *App. Math. Model.* **110:**172-192

[16] Hirani, A.N., Nakshatrala, K.B., Chaudhry, J.H., 2015. Numerical Method for Darcy Flow Derived Using Discrete Exterior Calculus. *Int. J. for Comp. Meth. In Eng. Sci. and Mech.* **16:**151-169

[17] Boom, P.D., Seepujak, A., Kosmas, O., Margetts, L., Jivkov, A.P., 2022. Parallelized discrete exterior calculus for three-dimensional elliptic problems. *Comp. Phys. Comm.* **279:**108456

[18] Boom, P.D., Kosmas, O., Margetts, L., Jivkov, A.P., 2022. A geometric formulation of linear elasticity based on discrete exterior calculus, *Int. J. of Solids & Struct.* **236**:111345

[19] Yavari, A., 2008. On geometric discretization of elasticity, *J. of Math. Phys.* **49**:022901.

[20] Smith, M., 2009. ABAQUS/Standard User's Manual, Version 6.9. *Dassault Systèmes Simulia Corp.*

[21] Von Mises, R., 1913. Mechanik der Festen Korper im Plastisch Deformablen Zustand. *Nachr. Ges. Wiss. Gottingen*,

1913:582-592.

[22] Reuss, A., 1930. Berucksichtigung der elastischen Formanderung in der Plastizitatstheorie, *Z. Angew. Math. Mech.* **10:**266-274

[23] Drucker, D. C., Prager, W., 1952. Soil mechanics and plastic analysis for limit design. *App. Math.* **10(2):**157–165.

[24] Mohamed, M.S., Hirani, A.N., Samtaney, R., 2016. Discrete exterior calculus discretization of incompressible Navier–Stokes equations over surface simplicial meshes. *J. Comp. Phys.* **312:**175-191

[25] Quey, R., Dawson, P.R., Barbe, F., 2011. Large-scale 3D random polycrystals for the finite element method: Generation, meshing and remeshing. *Comput. Methods Appl. Mech. Eng.* **200:**1729–1745.